Stability Analysis of Distributed Power Generation with Droop Inverters

Chung-Ching Chang, *Member, IEEE,* Dimitry Gorinevsky, *Fellow, IEEE,* and Sanjay Lall, *Fellow, IEEE*

Abstract—This paper models and analyzes a power distribution system with sources connected through inverters. The stabilizing effect of generator rotational inertia is emulated through inverter droop control logic. We model the nonlinear dynamics of the system with multiple distributed droop inverters using dynamical phasors. Linearizing the system around the steady-state we construct closed-loop transfer functions from exogenous disturbances to system states. This allows to evaluate the load disturbance impact on the inverter power and line voltage profile. As an example, the distribution system with 150 inverters is used to illustrate the approach.

Index Terms—Control systems, power distribution, power system stability, power system control, inverters.

I. INTRODUCTION

THE existing electrical grid was designed for centralized power generation, where the rotational energy of large synchronous generators is used to balance the instantaneous difference between the bulk supply and the demand. The primary governors of the generators stabilize the rotation frequency. The distribution systems are passive, and the voltage profile along a distribution line is a consequence of the power flow from the feeder to the loads.

Emerging distribution systems with distributed energy resources (DER) challenge this paradigm. Solar, battery, and other DER are connected through inverters that do not have the benefit of the intrinsic stabilizing effect of the rotational inertia. Currently, most inverters in the distribution systems use *grid-tie* control, where frequency and power are not linked. This is prescribed by the IEEE 1547 interconnect standard under the assumption that DER will provide for a small fraction of the total demand.

The need to support much greater penetration of renewables has led to the introduction of *droop* inverters, that emulate the response of generators with rotational inertia with control logic. The droop control logic is software implementation of the relationship between real-power and frequency exhibited by a turbine generator and its primary control system. On the bulk generation side, the software-induced inertia is already included in the code for the wind farm generation [16]. Economies of the bulk generation afford deployment of wide area integrated control systems. However, DER inverters in the distribution systems are, at present, controlled independently,

C.-C. Chang was with the Department of Electrical Engineering, Stanford University, Stanford, CA 94305, USA. He is now with Google Inc., Mountain View, CA 94043, USA (e-mall: ccchang@google.com)

D. Gorinevsky, and S. Lall are with the Department of Electrical Engineering, Stanford University, Stanford, CA, 94305, USA. Email: {gorin, lall}@stanford.edu

without coordination from higher-level supervisory control system; this is the setup analyzed in this paper.

Droop inverters in a distribution system influence line frequency. Multiple independent inverters interact through the line frequency. This can provide some degree of load balancing in the system. Yet, these interactions may also have unintended consequences, such as excessive frequency swings, power sharing issues, or voltage profile variations. Surprisingly, there appears to be little literature analyzing these important issues.

There is substantial technical literature on detailed modeling for both voltage source inverters (VSI) and current source inverter (CSI). The detailed models are suitable for inverter-level analysis, they are hard to use for analysis on distribution system level. The difficulty of analyzing such models with many inverters is in computational complexity. Prior work is limited to simulation case studies of systems with only a few inverters [3], [12]–[14]. Simulating systems with hundreds of inverters is currently computationally infeasible.

An alternative to the simulation is to linearize the multi-inverter model and perform small-signal analysis, see [2], [5], [8], [10], [17], [19]. The analysis of distribution systems with multiple inverters is commonly focused on the droop logic and inverter interaction. The internal inverter dynamics are left out and the inverters are modeled as ideal voltage sources with output impedances, see [2], [8], [10], [17]–[19]. The voltage source model effectively considers the inner-loop dynamic of the voltage/current controllers to be much faster than the outer-loop droop control logic, see [11]. The model order reduction can be formally justified through the singular perturbation analysis, e.g., see [15].

The goal of this paper is to analyze how deploying many DER droop inverters might affect the disturbance sensitivity of the distribution system. Most of the prior droop control analysis has been limited to closed-loop stability. In [6], the authors analyzed frequency and voltage stability. The analyzis in [2], [10] inlcuded power transients. A closed-loop stability criterion for a single droop inverter was developed in [8].

The prior work in analysis of disturbance rejection is limited to the load sharing for two droop inverters in [17] and [18]. This paper analyzes the disturbance rejection of a distribution system with many inverters. We generalize the ideal voltage source models used earlier to such setup. Section V shows that, for a single inverter example, our stability analysis results match [8] and our load sharing analysis matches [18].

The main contributions of this paper are as follows. First, we extend the modeling and small-signal analysis approach to distribution systems with many droop inverters. Our approach allows evaluation of the system stability and its sensitivity to

disturbances in frequency, load, and voltage profile. Second, we apply our approach to an example distribution system with 150 inverters spread along the line. We build the system model and analyze the voltage profile sensitivity to the distributed generation disturbances. The example illustrates how our approach can be used in engineering of power distribution systems with a large fraction of inverter-connected generation.
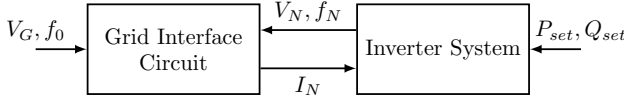
II. DROOP CONTROL

Fig. 1. Interconnection between an inverter and the distribution system

A basic model of the interconnection between the distribution system and an inverter is shown in Figure 1. This high-level model shows the information flow between two connected blocks: the Grid Interface Circuit and the Inverter System. The inverter system receives a measurement of the current I_N from the grid interface circuit and generates the interconnect voltage V_N with frequency f_N in the circuit. We consider a simplified single-phase AC circuit model where the grid voltage V_G, inverter voltage V_N, and inverter current I_N are phasors – complex variables describing the amplitudes and phases of the AC signals. The dynamic phasor analysis below considers the phasors as time-dependent complex variables.

In what follows, we consider the grid frequency f_G and inverter frequency f_N to be time varying, but close to the baseline frequency f_0 (60 Hz in the US). The time-varying frequencies are modeled throught the time-varying phases.

We use the following notation for phasors. For example, the inverter voltage V_N, may be represented as the sum of its real and imaginary parts as

$$V_N = \Re V_N + i \Im V_N,$$

or using its amplitude $|V_N|$ and phase angle ϕ_N as $V_N = |V_N| \angle \varphi_N$. Dynamic phasors are functions of time. For example, if $V_N = |V_N| \angle \varphi_N$ then

$$\frac{d}{dt} \varphi_N = 2\pi (f_N - f_0), \qquad (1)$$

where f_N is the instantaneous frequency of V_N.

Models for the grid interface circuit in Figure 1 are discussed in Sections III and IV.

The inverter system in Figure 1 is driven by control logic that receives active and reactive power setpoints P_{set}, Q_{set} (real numbers), current phasor measurement I_N, and generates the voltage V_N in accordance with the droop control law. The inverter is, thus, modeled as a voltage source with voltage magnitude and frequency controlled by the droop equations.

This paper considers two alternative droop control laws, called *conventional droop* and *opposite droop*. In conventional droop, we have the following relationships

$$\begin{aligned} f_N &= f_0 - K_f (P_N - P_{\text{set}}), \\ |V_N| &= V_{N,0} - K_V (Q_N - Q_{\text{set}}), \end{aligned} \qquad (2)$$

where the active power of the inverter P_N and the reactive power Q_N are related through

$$P_N + iQ_N = V_N I_N^*. \qquad (3)$$

An inverter would generally have an inner voltage feedback loop that measures P_N and Q_N in (3) and feeds it back into the voltage control law (2). In this paper we model it as an algebraic loop that is resolved as a part of the closed-loop analysis. A more detailed model can be found in [5].

The setpoint P_{set} in (2) is usually governed by the available output power, such as the maximum available power of a solar panel connected to the inverter. The reactive power is typically set to $Q_{\text{set}} = 0$. The gain K_f in (2) is typically chosen such that f_N is within the frequency range for any $P_N \in [0, P_{max}]$, where P_{max} is the maximum real output power of the inverter. The gain K_V is typically chosen such that V_N is within the voltage range for any $Q_N \in [-Q_{max}, Q_{max}]$, where Q_{max} is the maximum reactive output power of the inverter. The IEEE 1547 Standard [1] defines the acceptable frequency and voltage ranges. The setting $V_{N,0}$ in (2) could come from cascaded logic, such as a voltage control algorithm. For now, we assume $V_{N,0}$ is a constant that equals the nominal value of $|V_G|$, which would typically be 120V.

An alternative droop control law called *opposite droop* defines the output voltage according to

$$\begin{aligned} f_N &= f_0 - K_f (Q_N - Q_{\text{set}}), \\ |V_N| &= V_{N,0} - K_V (P_N - P_{\text{set}}). \end{aligned} \qquad (4)$$

Here, gains K_f and K_V are chosen such that f_N, V_N, P_N, and Q_N are in feasible ranges.

In this work, we choose the gains for the droop controller as follows

$$\begin{aligned} K_f &= \min \left(\frac{f_{N,\max} - f_0}{P_{\text{set}} - P_{N,\min}}, \frac{f_0 - f_{N,\min}}{P_{N,\max} - P_{\text{set}}} \right), \\ K_V &= \min \left(\frac{|V_N|_{\max} - V_{N,0}}{Q_{\text{set}} - Q_{N,\min}}, \frac{V_{N,0} - |V_N|_{\min}}{Q_{N,\max} - Q_{\text{set}}} \right). \end{aligned} \qquad (5)$$

For the opposite droop controller, we take

$$\begin{aligned} K_f &= -\min \left(\frac{f_{N,\max} - f_0}{Q_{N,\max} - Q_{\text{set}}}, \frac{f_0 - f_{N,\min}}{Q_{\text{set}} - Q_{N,\min}} \right), \\ K_V &= \min \left(\frac{|V_N|_{\max} - V_{N,0}}{P_{\text{set}} - P_{N,\min}}, \frac{V_{N,0} - |V_N|_{\min}}{P_{N,\max} - P_{\text{set}}} \right), \end{aligned} \qquad (6)$$

where P_{set} and Q_{set} are given and the sign of K_f and K_V can be determined as shown in the example in Section V-A. Taking the minimum here guarantees that the voltage and frequency are in their allowable ranges under all load settings.

Although many papers on the subject focus on conventional droop control, the results of this paper suggest that the inverters in distribution system should, in fact, use opposite droop control.

The model described here idealizes both the measurement and actuation circuits of an inverter. The measurements are assumed to be immediate without any delay, and the actuation circuit is modeled as an ideal voltage source. A more detailed and realistic model is considered in our paper [5]. Related work for a grid-tie inverter can be found in [9].

III. Single Inverter Circuit

A simple model of a single inverter in a distribution system is shown in Figure 2. The grid-connected feeder is represented by a constant voltage source V_G with infinite capacity.
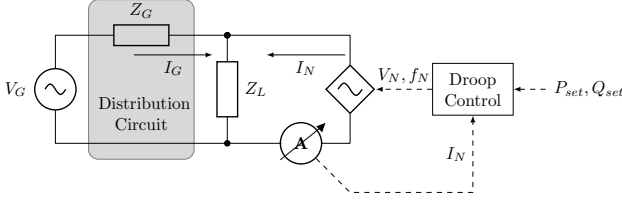

Fig. 2. Single inverter model

Our reduced-order phasor model neglects the dynamic of the distribution circuit. This makes it more scalable. As discussed in [11], this is acceptable for a slow system; in our case the distribution system is stabilized by the high inertia of the connected grid. In this model, the grid interface circuit includes an aggregated load with impedance $Z_L \in \mathbb{C}$ and the distribution circuit with impedance $Z_G \in \mathbb{C}$. The impedances Z_L and Z_G are equivalent impedances as seen from the low voltage circuit and include the medium voltage line impedances. The line impedance is proportional to the line distance. We assume that the inverter is located much closer to the load than the feeder and, therefore, that the impedance between the inverter and the load can be neglected.

We are interested in how V_N, f_N, P_N, and Q_N respond to disturbances such as changes in the load and inverter power setpoint.

A. Steady-State Solution

The complex load power $P_L + iQ_L$ can be computed as

$$P_L + iQ_L = V_N(I_G + I_N)^*$$
$$= (P_N + iQ_N) + (P_G + iQ_G), \qquad (7)$$

where the line current I_G is related to V_G and V_N through the distribution circuit model in Figure 2. We have

$$I_G = \frac{V_G - V_N}{Z_G}. \qquad (8)$$

The grid-provided power $P_G + iQ_G$ in (7) is defined as

$$P_G + iQ_G = V_N I_G^*. \qquad (9)$$

Without loss of generality, we may assume $V_G = 120\angle 0$, since all circuit equations hold when we shift all phasors by a constant phase. This corresponds to a change in the reference time. Substituting I_G from (8) into (9) gives

$$P_G + iQ_G = \frac{|V_N||V_G|\angle\varphi_N}{Z_G^*} - \frac{|V_N|^2}{Z_G^*}. \qquad (10)$$

Equations (1), (2), (7), and (10) describe the nonlinear closed-loop dynamics for the conventional droop controller as shown in Figure 3.

In steady-state, $f_G = f_N = f_0$. Assuming that V_G, Z_G, K_f, K_V, V_{N_0}, f_0, P_L, Q_L, P_{set}, and Q_{set} are given, the nonlinear equations (2), (7), and (10) can be solved numerically to find
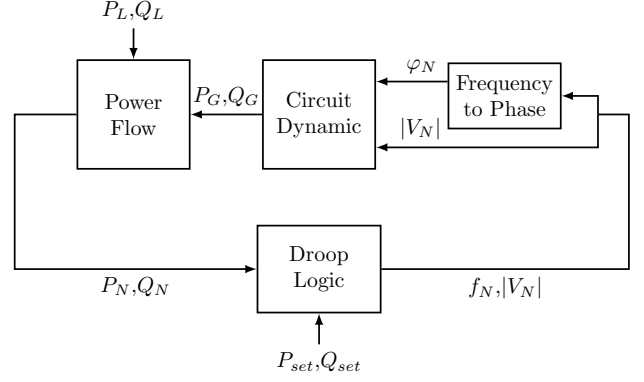

Fig. 3. Closed-loop control

P_N, Q_N, P_G, Q_G, V_N, and I_N. Note that there are 6 real equations and 6 unknowns.

Equations (2) and (7) are linear and bijective for appropriate K_V and K_f. The only closed-loop system nonlinearity lies in (10). We remove the nonlinearity in $\angle\varphi_N$ using the fact that $(\sin\varphi_N)^2 + (\cos\varphi_N)^2 = 1$. By rearranging, taking squares of the real and imaginary parts in (10), and adding them, we form a fourth-order polynomial equation in $|V_N|$, which can be solved numerically. The rest of the unknowns can be then calculated. A detailed discussion of the computation of the steady state solution is outside of the limited scope of this paper. A derivation of the steady state solution for a closely related power system can be found in [9].

B. Transient Dynamics and Disturbance Rejection

In what follows, we analyze perturbations of the nonlinear closed-loop system around its steady-state. We linearize the nonlinearity in (10) as follows.

Let $|V_N| = |V_G| + v$. The solution can be simplified by noticing that, because the line impedance is small (power losses are small), we must have $v \ll |V_G|$. For the same reason, in (10) we have $|\varphi_N| \ll 1$ and

$$1\angle\varphi_N \approx 1 + i\varphi_N. \qquad (11)$$

Let $Z_G = R_G + iX_G$. Since $|\varphi_N|$ is small, we have

$$P_G = -\frac{|V_N|^2 R_G}{|Z_G|^2} + \frac{|V_N||V_G|}{|Z_G|^2}(R_G - X_G\varphi_N),$$
$$Q_G = -\frac{|V_N|^2 X_G}{|Z_G|^2} + \frac{|V_N||V_G|}{|Z_G|^2}(X_G + R_G\varphi_N).$$

Replacing $|V_N|$ by $|V_G| + v$, and keeping only the zeroth and first order terms in v and φ_N, we have

$$P_G = -\frac{R_G|V_G|}{|Z_G|^2}v - \frac{X_G|V_G|^2}{|Z_G|^2}\varphi_N,$$
$$Q_G = -\frac{X_G|V_G|}{|Z_G|^2}v + \frac{R_G|V_G|^2}{|Z_G|^2}\varphi_N. \qquad (12)$$

Using the linearized model (12), we form the corresponding transient model around its steady-state. For small signal

perturbations in (12), we have

$$\begin{bmatrix} \delta P_G \\ \delta Q_G \end{bmatrix} = A \begin{bmatrix} \delta v \\ \delta \varphi_N \end{bmatrix}, \qquad (13)$$

$$A = -\frac{|V_G|}{|Z_G|^2} \begin{bmatrix} R_G & X_G|V_G| \\ X_G & -R_G|V_G| \end{bmatrix}. \qquad (14)$$

From (7), we have the transient

$$\begin{bmatrix} \delta P_L \\ \delta Q_L \end{bmatrix} = \begin{bmatrix} \delta P_N \\ \delta Q_N \end{bmatrix} + \begin{bmatrix} \delta P_G \\ \delta Q_G \end{bmatrix}. \qquad (15)$$

Using (1), (2), and $V_{N,0} = |V_G|$, yields

$$\begin{bmatrix} \delta v \\ \delta \varphi_N \end{bmatrix} = C \begin{bmatrix} \delta P_N \\ \delta Q_N \end{bmatrix} - C \begin{bmatrix} \delta P_{\text{set}} \\ \delta Q_{\text{set}} \end{bmatrix}. \qquad (16)$$

For conventional droop we have

$$C = \begin{bmatrix} 0 & -K_V \\ -\frac{2\pi}{s} K_f & 0 \end{bmatrix} \qquad (17)$$

and for opposite droop, we have

$$C = \begin{bmatrix} -K_V & 0 \\ 0 & -\frac{2\pi}{s} K_f \end{bmatrix}. \qquad (18)$$

Equations (13), (15), and (16) define a linearized closed-loop model with exogenous disturbances δP_L, δQ_L, δP_{set}, and δQ_{set}. The closed-loop responses to these exogenous disturbances are presented below.

a) Load power disturbance.: For $\delta P_{\text{set}} = 0$ and $\delta Q_{\text{set}} = 0$, we have

$$\begin{bmatrix} \delta P_N \\ \delta Q_N \end{bmatrix} = (I + AC)^{-1} \begin{bmatrix} \delta P_L \\ \delta Q_L \end{bmatrix}, \qquad (19)$$

where A is defined in (13) and C is defined in (17) or (18). Based on (16), the voltage deviation is given by

$$\delta v = \begin{bmatrix} 1 & 0 \end{bmatrix} C(I + AC)^{-1} \begin{bmatrix} \delta P_L \\ \delta Q_L \end{bmatrix}. \qquad (20)$$

b) Power setpoint disturbance.: For $\delta P_L = 0$ and $\delta Q_L = 0$, we have

$$\begin{bmatrix} \delta P_N \\ \delta Q_N \end{bmatrix} = (I + AC)^{-1} AC \begin{bmatrix} \delta P_{\text{set}} \\ \delta Q_{\text{set}} \end{bmatrix}. \qquad (21)$$

Based on (16), the voltage deviation is given by

$$\delta v = - \begin{bmatrix} 1 & 0 \end{bmatrix} C(I + AC)^{-1} \begin{bmatrix} \delta P_{\text{set}} \\ \delta Q_{\text{set}} \end{bmatrix}. \qquad (22)$$

The derived transfer functions (19) and (20), where matrices A and C are given by (14) and (17) or (18), allow us to analyze how the power and voltage supplied by the inverter respond when load changes. Similarly, equations (21) and (22) allow us to analyze how the power and voltage respond to inverter power setpoint changes. We discuss this model in more detail for an example system in Section V-A.

IV. MULTIPLE INVERTERS

A model of a distribution system with multiple inverters is illustrated in Figure 4. The feeder is shown as the voltage source V_G with infinite capacity. The shaded box shows the distribution circuit combining Medium Voltage (MV) and Low Voltage (LV) power distribution circuits. The analysis of this section is applicable to any linear distribution circuit. An example circuit with a linear topology is shown in Figure 6.
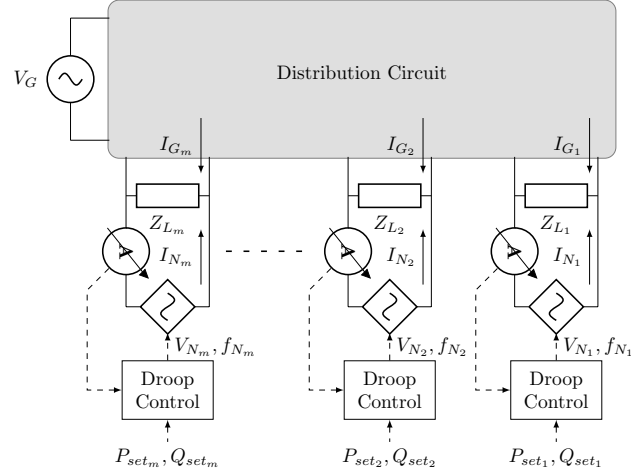

Fig. 4. Circuit with multiple inverters

A. System Model and Notation

In our model, the distribution system serves m customers. Customer k is modeled by an aggregate load with impedance $Z_{L_k} \in \mathbb{C}$. Customer k has an inverter modeled by an ideal voltage source V_{N_k} with frequency f_{N_k}. The droop controller of the inverter computes V_{N_k}, f_{N_k} based on power setpoints $P_{\text{set}_k}, Q_{\text{set}_k}$, and current measurement I_{N_k}. Inverter k generates real and reactive power P_{N_k} and Q_{N_k}. Customer k draws current I_{G_k} from the distribution circuit.

We use notation similar to that used for the single inverter case of Section III, with a subscript $k = 1, 2, \ldots, m$ to indicate the customer. In the single inverter model, equations (1), (2), (7), and (10) describe the nonlinear closed-loop dynamics. In the multiple inverter problem, (1) is replaced by

$$\frac{d}{dt} \varphi_{N_k} = 2\pi(f_{N_k} - f_0), \qquad (23)$$

and for conventional droop equation (2) is replaced by

$$\begin{aligned} f_{N_k} &= f_0 - K_{f_k}(P_{N_k} - P_{\text{set}_k}), \\ |V_{N_k}| &= V_{N_k,0} - K_{V_k}(Q_{N_k} - Q_{\text{set}_k}), \end{aligned} \qquad (24)$$

where K_{f_k} and K_{V_k} are the droop parameters for inverter k. This paper assumes $V_{N_k,0} = 120V$. For inverter k, matrix C in (17) is replaced by C_k with droop gains K_{f_k} and K_{V_k}. For opposite droop, (18) is changed in a similar way. For the multiple inverter model, we define the vector

$$\bar{V}_N = \begin{bmatrix} V_{N_1} & V_{N_2} & \ldots & V_{N_m} \end{bmatrix}^T$$

and similarly for $\bar{I}_N$, $\bar{I}_G$, $\bar{Z}_{MV}$, $\bar{Z}_{LV}$, $\bar{P}_G$, and $\bar{Q}_G$.

B. Steady-State Solution

In multiple inverter case, equations (7), (3), and (9) take the form

$$P_{L_k} + iQ_{L_k} = (P_{N_k} + iQ_{N_k}) + (P_{G_k} + iQ_{G_k}), \qquad (25)$$

$$P_{N_k} + iQ_{N_k} = V_{N_k} I_{N_k}^*, \qquad (26)$$

$$P_{G_k} + iQ_{G_k} = V_{N_k} I_{G_k}^* \qquad (27)$$

Since the distribution circuit model is linear, the simple inverter circuit model (8) will be replaced by a linear circuit

map T_{ckt} from $\bar{V}_N$ and V_G to $\bar{I}_G$. This map depends on the topology of the distribution circuit. One could use mesh analysis [4] or tableau analysis to derive map T_{ckt} for a circuit. This linear map can be presented in the form

$$\bar{I}_G = X\bar{V}_N + YV_G, \tag{28}$$

where the entries of the complex matrices X and Y can be found from the circuit model. An example of this is presented in Section VI-A.

Combining (27) and (28), we have a multiple inverter formula corresponding to (10).

$$
\begin{aligned}
P_{G_k} + iQ_{G_k} &= \left(x_k^T \bar{V}_N + y_k V_G\right)^* V_{N_k} \\
&= \begin{bmatrix} (x_k^T)^* & y_k^* \end{bmatrix} \begin{bmatrix} \bar{V}_N^* V_{N_k} \\ V_G^* V_{N_k} \end{bmatrix},
\end{aligned} \tag{29}
$$

where x_k^T is the k-th row of X and y_k is the k-th entry of Y.

Equations (23), (24), (25), and (29) describe the nonlinear dynamics of the multiple inverter distribution system. The closed-loop control blocks are connected similar to Figure 3; there are now m control loops coupled by the circuit dynamic (29). The scalar signal P_G is replaced by the vector signal $\bar{P}_G$

The steady-state could be analyzed in a similar way to the single inverter case in Section III. In this work, we compute the steady-state solution for the multiple inverter problem numerically, as described in Section VI-A.

C. Transient Dynamics and Disturbance Rejection

In this section we linearize the nonlinear system using an approach similar to that used for the single inverter case. We will assume $|V_{N_k}| = |V_G| + v_k$ for all k.

Assuming small power losses in the distribution circuit, we must have $v_i \ll |V_G|$ for all i, and $|\varphi_{N_k} - \varphi_{N_j}|$ and $|\varphi_{N_k}|$ small for all k, j. Thus, we can linearize the phases in $\bar{V}_N^* V_{N_k}$ and $\bar{V}_N V_G^*$ similar to (11), and then neglect the second order terms in the variables v_i, $\varphi_{N_j} - \varphi_{N_k}$, and φ_{N_l} for any $i, j, k, l \in \{1, 2, \ldots, m\}$. With this assumption, both $\bar{V}_N^* V_{N_k}$ and $V_G^* V_{N_k}$ become (complex) affine in $\begin{bmatrix} v_k \\ \varphi_{N_k} \end{bmatrix}$ for all k. Since $P_{G_k} + iQ_{G_k}$ is linear in $\bar{V}_N^* V_{N_k}$ and $V_G^* V_{N_k}$, it is affine in $\begin{bmatrix} v_k \\ \varphi_{N_k} \end{bmatrix}$. Hence we have for each k the linear map

$$\begin{bmatrix} P_{G_k} \\ Q_{G_k} \end{bmatrix} = \sum_{k=1}^{m} A_{kj} \begin{bmatrix} v_j \\ \varphi_{N_j} \end{bmatrix} + W_k. \tag{30}$$

Real matrices A_{kj} are obtained by linearization of (29). Matrix A_{kj} is analogous to A in (14), with matrices A_{kj} defined by the responses at different points in the circuit to the changes in the voltage v_j and phase at the φ_{N_j} interconnect of inverter j. Computation of A_{kj} is further discussed for a specific circuit example in Section (VI-A). Real matrices W_k give the intercept of the linearization and are defined by the steady state solution discussed in Subsection IV-B.

We can aggregate (30) into the vector form

$$\overline{\begin{bmatrix} P_G \\ Q_G \end{bmatrix}} = \bar{A} \overline{\begin{bmatrix} v \\ \varphi_N \end{bmatrix}} + \bar{W},$$

$$
\bar{A} = \begin{bmatrix} A_{11} & A_{12} & \cdots & \\ A_{21} & A_{22} & \cdots & \\ \vdots & \vdots & \ddots & \vdots \\ & & \cdots & A_{mm} \end{bmatrix}
\qquad
\bar{W} = \begin{bmatrix} W_1 \\ W_2 \\ \vdots \\ W_m \end{bmatrix}
$$

$$\overline{\begin{bmatrix} v \\ \varphi_N \end{bmatrix}} = \begin{bmatrix} v_1 & \varphi_{N_1} & \cdots & v_m & \varphi_{N_m} \end{bmatrix}^T$$

$$\overline{\begin{bmatrix} P_G \\ Q_G \end{bmatrix}} = \begin{bmatrix} P_{G_1} & Q_{G_1} & \cdots & P_{G_m} & Q_{G_m} \end{bmatrix}^T$$

We use similar notation for

$$\overline{\begin{bmatrix} \delta P_G \\ \delta Q_G \end{bmatrix}}, \quad \overline{\begin{bmatrix} \delta P_N \\ \delta Q_N \end{bmatrix}}, \quad \overline{\begin{bmatrix} \delta P_L \\ \delta Q_L \end{bmatrix}}, \quad \overline{\begin{bmatrix} \delta P_{\text{set}} \\ \delta Q_{\text{set}} \end{bmatrix}}, \quad \overline{\begin{bmatrix} \delta v \\ \delta \varphi_N \end{bmatrix}}$$

Recall that (13), (15), and (16) fully characterize the linearized closed-loop system in the single inverter problem. For the multiple inverter problem, the replacements for (15) and (16), derived from (25), (24) and (23), are

$$\overline{\begin{bmatrix} \delta P_L \\ \delta Q_L \end{bmatrix}} = \overline{\begin{bmatrix} \delta P_N \\ \delta Q_N \end{bmatrix}} + \overline{\begin{bmatrix} \delta P_G \\ \delta Q_G \end{bmatrix}}, \tag{31}$$

$$\overline{\begin{bmatrix} \delta v \\ \delta \varphi_N \end{bmatrix}} = \bar{C} \overline{\begin{bmatrix} \delta P_N \\ \delta Q_N \end{bmatrix}} - \bar{C} \overline{\begin{bmatrix} \delta P_{\text{set}} \\ \delta Q_{\text{set}} \end{bmatrix}}, \tag{32}$$

$$\bar{C} = \text{block diag}\{C_1, \ldots, C_m\}, \tag{33}$$

where $C_1, \ldots, C_m$ are gain matrices of the form (17) for droop controllers, with the gains from (24). For opposite droop controllers, we have $C_1, \ldots, C_m$ of the form (18).

For multiple inverters, the generalization of the transient map (13) is

$$\overline{\begin{bmatrix} \delta P_G \\ \delta Q_G \end{bmatrix}} = \bar{A} \overline{\begin{bmatrix} \delta v \\ \delta \varphi_N \end{bmatrix}}. \tag{34}$$

The closed-loop dynamics of the linearized system are then given by (31), (32), and (34). These equations allow analysis of the impacts of disturbances to load power, power setpoint, and grid frequency, following the method used in Section III. For example, the power setpoint disturbance responses (21) and (22) are changed to

$$\overline{\begin{bmatrix} \delta P_N \\ \delta Q_N \end{bmatrix}} = (I + \bar{A}\bar{C})^{-1} \bar{A}\bar{C} \overline{\begin{bmatrix} \delta P_{\text{set}} \\ \delta Q_{\text{set}} \end{bmatrix}}, \tag{35}$$

$$\overline{\delta v} = -\left(I \otimes \begin{bmatrix} 1 & 0 \end{bmatrix}\right) \bar{C}(I + \bar{A}\bar{C})^{-1} \overline{\begin{bmatrix} \delta P_{\text{set}} \\ \delta Q_{\text{set}} \end{bmatrix}}, \tag{36}$$

where $\otimes$ is the matrix Kronecker product $\bar{A}$ is as in (34) and $\bar{C}$ is as in (32).

V. SINGLE INVERTER EXAMPLE

Following the formulation in Section III, we show that this model complies with the stability analysis in [8] in Section V-A. The disturbance rejection result in Section V-B shows that the opposite droop is preferred in the low voltage grid in terms of load-sharing and voltage control, which complies with the result in [18] from the perspective of line power loss.

A. Single-Inverter Model

Consider a scenario in which a single residential customer in a rural area is served with 10kVA through a main feeder with 2.4kV, AWG #3/0 for 2km, which is then stepped down to 120V with AWG #3 for the last 20m. A rooftop photovoltaic system with a 5kW rating is connected through a droop inverter at 120V. Suppose the steady-state load power factor is 0.98. We consider here how the system would respond to increases in the load.

We start by applying the theoretical analysis for the single inverter problem introduced in Section III. In this example, we assume $R_G \gg X_G$. This is often a good approximation. Transfer functions (19) and (20) for the case of conventional droop then become

$$\begin{bmatrix} \delta P_N \\ \delta Q_N \end{bmatrix} = \frac{1}{s + \frac{2\pi |V_G|^3 K_V K_f}{R_G^2}} \begin{bmatrix} s & -\frac{|V_G| K_V s}{R_G} \\ \frac{2\pi |V_G|^2 K_f}{R_G} & s \end{bmatrix} \begin{bmatrix} \delta P_L \\ \delta Q_L \end{bmatrix}$$

and

$$\delta v = \frac{1}{s + \frac{2\pi |V_G|^3 K_V K_f}{R_G^2}} \begin{bmatrix} -\frac{2\pi |V_G|^2 K_f K_V}{R_G} & -K_V s \end{bmatrix} \begin{bmatrix} \delta P_L \\ \delta Q_L \end{bmatrix}.$$

These transfer functions show that the closed-loop system has poles with negative real part, and is therefore stable, when $K_V K_f > 0$. This condition matches the results of [8].

However, the closed-loop response to load changes for the conventional droop is not desirable. This can be seen from the steady-state values of the step responses (the closed-loop transfer functions at $s = 0$). When δP_L increases, δP_N does not increase to compensate for the change, while instead δQ_N and δv change with a possibly undesirable sign. Further, the inverter does not respond when δQ_L changes.

In the case of opposite droop, when $R_G \gg X_G$, equations (19) and (20) yield

$$\begin{bmatrix} \delta P_N \\ \delta Q_N \end{bmatrix} = \begin{bmatrix} \left(1 + \frac{|V_G|}{R_G} K_V\right)^{-1} & 0 \\ 0 & \left(1 - \frac{2\pi |V_G|^2 K_f}{R_G s}\right)^{-1} \end{bmatrix} \begin{bmatrix} \delta P_L \\ \delta Q_L \end{bmatrix},$$

$$\delta v = \begin{bmatrix} -\frac{K_V}{1 + K_V |V_G|/R_G} & 0 \end{bmatrix} \begin{bmatrix} \delta P_L \\ \delta Q_L \end{bmatrix}.$$

In this case the closed-loop system is stable when $K_f < 0$ and $K_V \neq -\frac{R_G}{|V_G|}$. Again, the inverter does not respond when δQ_L changes. However, when δP_L increases, δP_N compensates for the change if $K_V > 0$. This means the opposite droop provides better power sharing than the conventional droop.

B. Single-Inverter Disturbance Response

Using reference data from [7], the line impedances are $0.2627 + i0.1378$ Ω/km for the MV line and $0.7972 + i0.1056$ Ω/km for the LV lines. The overall impedance is given by $Z_G = 0.0173 + i0.0028$ Ω as seen from the LV grid. Since the load is 10kVA with power factor 0.98, we have $P_L = 9.8$kW and $Q_L = 1.99$kVars. We choose $K_f = 1.4 \times 10^{-4}$ and $K_V = 3.9 \times 10^{-3}$ for the conventional droop inverter. We take $f_0 = 60$, $V_{N,0} = 120$, and $P_{set} = 5000 \times \frac{0.5}{0.5 + 0.2}$. In accordance with (5) in Section II, we must have $K_f \leq 1.4 \times 10^{-4}$

to ensure $f_N \in [59.8, 60.5]$ Hz for $P_N \in [0, 5000]$. Since the power factor is at least 85% in steady-state, $|Q_N|$ may not exceed $3100 = 5000 \tan(\cos^{-1} 0.85)$. We choose $K_V > 0$ such that $|V_N|/V_{N,0} \in [0.88, 1.1]$ for $Q_N \in [-3100, 3100]$. Similarly, we choose $K_f = -4.1 \times 10^{-5}$ and $K_V = 3.4 \times 10^{-3}$ for the opposite droop inverter.

According to our analysis, a unit step in δP_L yields $\delta Q_N = 0.043$ and $\delta v = -1.44 \times 10^{-4}$ for conventional droop and $\delta P_N = 0.041$ and $\delta v = -1.38 \times 10^{-4}$ for the opposite droop case. A step in δQ_L does not have any effect in either case. The computed values are defined by on R_G, $|V_G|$, and K_V. The responses to the load changes are illustrated in Figure 5.
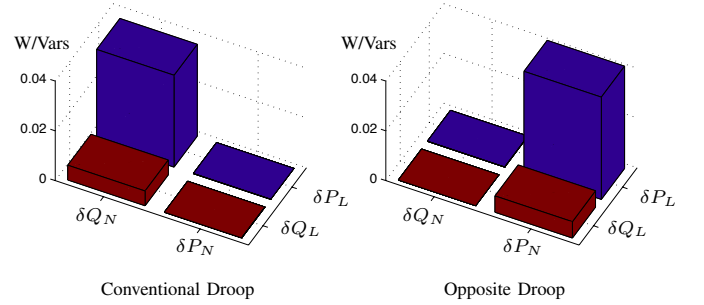

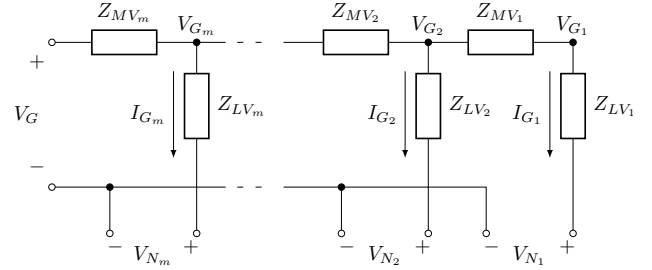Fig. 5. Load power disturbance with a single inverter

Fig. 6. Distribution circuit

VI. MULTIPLE INVERTER EXAMPLE

We apply the formulation in Section IV specifically to the line topology in Figure 6. We analyzed the voltage profile deviation along the distribution line spatio-temporally when power setpoints of inverters change, for example, due to the change in the perception of the solar panels. We show that it is feasible to analyze dynamic disturbance rejection of a distribution system with hundred houses on a laptop.

A. Multiple-Inverter Model

As an example of a system with multiple inverters, consider the distribution circuit with the linear topology in Figure 6. The line impedances are Z_{MV_k} and the connection impedances are Z_{LV_k}. In practice, Z_{MV_k} would include the equivalent MV grid impedance as seen from the LV grid. This example assumes that all inverters are identical, apart from their setpoints.

To apply the analysis of Section IV, we build a linear map of the form of equation (28) for the distribution circuit in

Figure 6. A model of this circuit is

$$\left(V_{N_{k+1}} + Z_{LV_{k+1}}I_{G_{k+1}}\right) - (V_{N_k} + Z_{LV_k}I_{G_k})$$
$$= Z_{MV_k}\sum_{j=1}^{k}I_{G_j}, \quad (37)$$

where the quantities on the left-hand-side are the voltage drops over the impedances Z_{MV_k}. The currents I_{G_k} on the right-hand-side are determined by the KCL. This holds for $k = 1, 2, \ldots, m-1$. The boundary condition for $k = m$ is

$$V_G - (V_{N_m} + I_{G_m}Z_{LV_m}) = Z_{MV_m}\sum_{j=1}^{m}I_{G_j}. \quad (38)$$

Equations (37) and (38) can be presented in form of (28) with $X = -\bar{R}^{-1}L^{-T}$ and $Y = \bar{R}^{-1}e_m$, where

$$\bar{R} = \text{diag}(\bar{Z}_{MV})L + (I - D^T)\,\text{diag}(\bar{Z}_{LV}), \quad (39)$$

and e_m is the m-th unit vector, I is the identity matrix, D is the unit shift matrix with 1 in the subdiagonal entries and 0 elsewhere, and $L^{-1} = I - D$.

The steady-state solution is calculated numerically. Starting with an initial approximation for V_{G_1}, we calculate I_{G_1} according to the fourth-order polynomial equation described in Section III-A. We then calculate V_{G_2} according to Ohm's law. By calculating V_{G_k} iteratively for increasing k, we finally reach V_G and compare $|V_G|$ with 120. If $|V_G|$ is close to 120, we multiply all voltage and current phasors by $1\angle V_G^*$. This results in $V_G = 120$ and ensures that the remaining equations still hold. In the multiple inverter case, system stability can be determined by examining the poles of the closed-loop transfer function $(I + \bar{A}\bar{C})^{-1}\bar{A}\bar{C}$ in (35).

According to IEEE 1547, we must have $v_i \ll |V_G|$ for all i, and power angles are regulated to be small. Thus, $|\varphi_{N_k}|$ is small for all k, j. As shown in the appendix, this leads to $|\varphi_{N_k} - \varphi_{N_j}|$ small as well.

Following the steps used in Section IV, we have (34) with

$$\bar{A} = \begin{bmatrix} \Re(g_1^*\Omega) \\ \Im(g_1^*\Omega) \\ \vdots \\ \Re(g_m^*\Omega) \\ \Im(g_m^*\Omega) \end{bmatrix}, \quad (40)$$

where g_k^* is the complex conjugate transpose of the k-th column of $G = \bar{R}^{-1}$ ($\bar{R}$ is given by (39)) and matrix Ω is

$$\Omega = L^{-1} \otimes \begin{bmatrix} -|V_G| & i|V_G|^2 \end{bmatrix}. \quad (41)$$

B. Multiple-Inverter Disturbance Response

In what follows, we exemplify the use of this model in an analysis of the system described in Section VI-A. We would like to determine the effect of disturbances to the power setpoint on the voltage profile. Figure 7 illustrates such a system with a linear topology. We consider a scenario where a cloud drifts through the area of the distribution system, shading the solar panels. Suppose the cloud shades 30 houses in a row. The cloud drifts from left to right with constant speed, entering
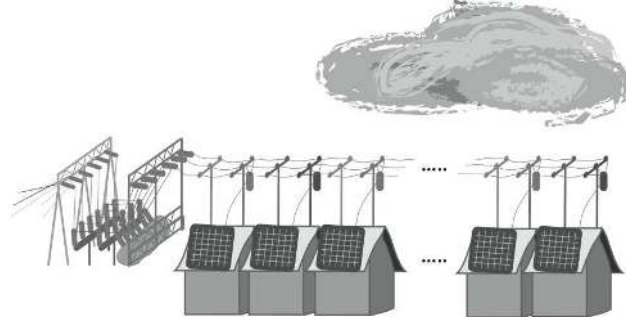

Fig. 7. A multiple inverter system with disturbances to the power set point

the area at $t = 0$s and leaving at $t = 89$s. We would like to determine how the voltage profile changes with the insolation.

We model the case where there is a substation serving a residential area through a main feeder (2.4kV, 3/0 AWG) for 7km. There are 150 houses equally spaced along the distribution line, each with 10kVA of load with power factor 0.98. The grid voltage steps down to 120V at the roadside poles and connects to each house with AWG #3 wire for the last 20m. Each house has a residential photovoltaic system rated at 5kW connected to the grid through a droop inverter.

The inverters are equipped with opposite droop control, as in the single inverter example of Section V-A with $K_f = -4.1 \times 10^{-5}$ and $K_V = 3.4 \times 10^{-3}$. Following the data of [7], we assume $Z_{MV_k} = (3.065 + i1.608) \times 10^{-5}$ and $Z_{LV_k} = 0.0159 + i0.0021$ for all $k = 1, 2, \ldots, 150$.

The analysis model was built according to the procedure of Section VI-A. Matrix $\bar{A}$ of equation (40) was computed in accordance with the distribution circuit model in Figure 6, where g_k is the k-th column of $G = R^{-1}$, Ω is as in (41), and the matrix $\bar{R}$ in equation (39) is formed using the above values for the parameters Z_{MV_k} and Z_{LV_k}. The matrix $\bar{C}$ of equation (33) was computed from (18) where the opposite droop controller gains for this example are given in (6). This allows computation of the transfer function $T_{vp} = -\left(I \otimes \begin{bmatrix} 1 & 0 \end{bmatrix}\right)\bar{C}(I + \bar{A}\bar{C})^{-1}$ in (36).

Using the closed-loop transfer function (36), we compute the steady-state step responses of the voltage profile at each point along the distribution line. This is plotted in Figure 8. The 3-D plot shows deviations of the voltage profile $(\delta|V_{G_1}|, \delta|V_{G_2}|, \ldots, \delta|V_{G_m}|)$ as a function of the line location, in response to steps in each of the active power setpoints δP_{set_k} for each k. Voltages V_{G_k} follow the notation in Figure 6. The solid line in Figure 8 highlights one specific voltage profile obtained by increasing $\delta P_{\text{set}_3 0}$ by 1kW. The profile is computed from the steady-state closed-loop map given by $T_{vp}(0)$, where T_{vp} is the closed-loop transfer function in (36). Figure 8 shows the entire matrix $T_{vp}(0)$, and includes the responses to each inverter active power change.

Figure 9 shows the step responses in δV_{G_1}, $\delta V_{G_{75}}$, and $\delta V_{G_{150}}$ when $\delta P_{\text{set}_3 0}$ increases by 1kW. The 1kW step in a single power setpoint results in a steady-state deviation on the order of 10mV in the distribution line. The effect of the local power change is absorbed by the entire system.

Figure 10 shows the voltage profile as the cloud drifts by.
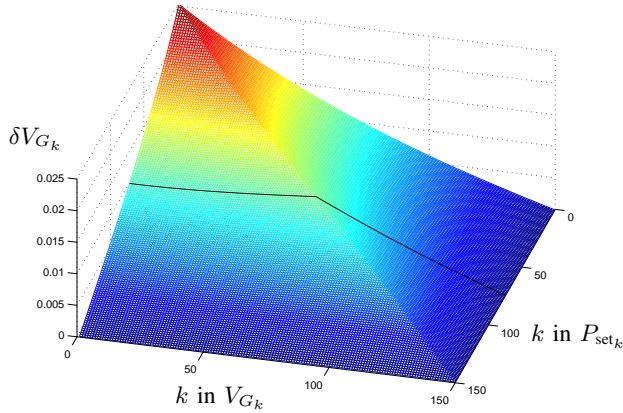
7

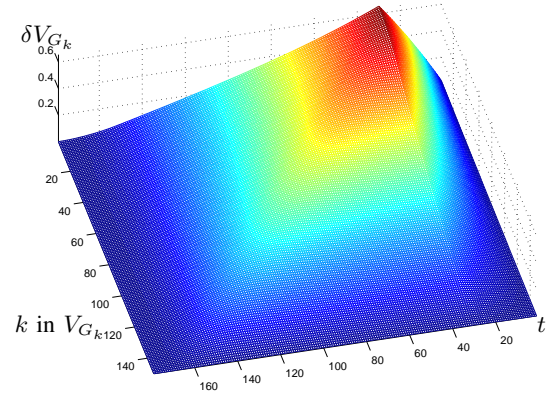Fig. 8. Voltage profile responses to disturbances in the power setpoint

Fig. 10. Voltage profile deviation due to shading by a passing cloud
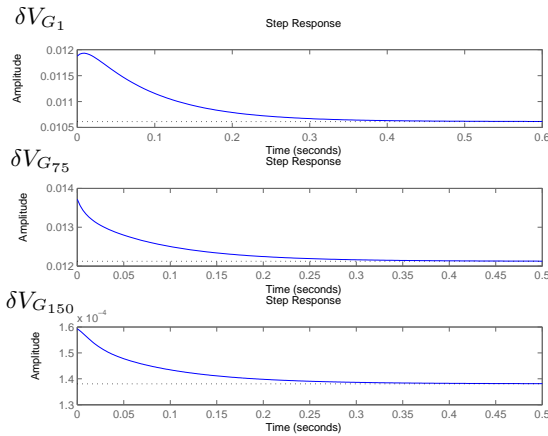

Fig. 9. Step responses to disturbances in the power setpoint

We assume that the power setpoint P_{set_k} of each inverter decreases by 1kW when the house is shaded. The maximum voltage deviation appears at node 1 at $t = 30$, with an amplitude of approximately 0.66V. The volatility of the voltage profile would be exacerbated for a more dense cloud. The result obtained here for a distribution system with a linear topology is consistent with the step responses in Figure 8. The same modeling and analysis approach can be applied to a distribution system with an arbitrary topology, where the voltage profile effects would be much less obvious. The presented methodology for analysis of the voltage profile response can therefore be used when choosing the margin for voltage profile in distribution system engineering.

VII. CONCLUSION

The linearized perturbation dynamics of an electric distribution system with single or multiple droop inverters is described by equations (13), (15) and (16) for a single inverter, and (31), (32) and (34) for multiple inverters. This perturbation model allows evaluation of the closed-loop disturbance rejection of the system according to (19) and (20) for load power disturbances, and (21), (22), (35), and (36) for power setpoint disturbances. The single inverter example in Section V

shows that opposite droop control outperforms conventional droop control in accommodating load power disturbances. The example of Section VI illustrates how the developed methodology can support analysis of the voltage profiles in power distribution systems.

The linearized analysis proposed in this paper outperforms traditional simulation-based analysis in several aspects. First, analysis of the linearized model is significantly faster than simulation. The linearized model analysis of the 150-inverter example in Section V is completed in a few seconds. Most of this time is spent on setting up the transfer functions, which needs to be done once when doing repeated analysis for different inputs. Next, since the model in this paper allows for multiple inverters, it can be used for analysis of spatio-temporal disturbances of the voltage and power flow in power distribution systems. Finally, the analysis method developed in this paper is more informative than performing simulations. The transfer function model allows analysis of the system performance using control theoretic techniques, which are often very powerful. For example, one may compute the H_∞ norm of a transfer function to determine the worst case disturbance rejection performance. The alternative of evaluating the worst case using simulations would require a large number of runs.

REFERENCES

[1] IEEE 1547. Interconnecting distributed resources with electric power systems. IEEE, 2003.

[2] H. J. Avelar, W. A. Parreira, J. B. Vieira Jr., L. C. Gomes de Freitas, and E. A. A. Coelho. A state equation model of a single-phase grid-connected inverter using a droop control scheme with extra phase shift control action. *IEEE Transactions on Industrial Electronics*, 59(3):1527–1537, 2012.

[3] S. Barsali, M. Ceraolo, P. Pelacchi, and D. Poli. Control techniques of dispersed generators to improve the continuity of electricity supply. In *IEEE Power Engineering Society Winter Meeting*, 2002.

[4] A. B. Carlson. *Circuits*. Brooks Cole, 2000.

[5] C.-C. Chang, D. Gorinevsky, and S. Lall. Dynamical and voltage profile stability of inverter-connected distributed power generation. *IEEE Transactions on Smart Grid*, 5(4):2093–2105, July 2014.

[6] E. A. A. Coelho, P. C. Cortizo, and P. F. D. Garcia. Small-signal stability for parallel-connected inverters in stand-alone ac supply systems. *IEEE Transactions on Industry Applications*, 38(2):533–542, 2002.

[7] General Electric Company. *Distribution Data Book: A Collection of Fundamental Data Pertaining to the Elements Of, and the Loads On, Distribution Systems*. General Electric Company, 1972.

[8] A. Engler. Applicability of droops in low voltage grids. *International Journal of Distributed Energy Resources*, 1(1):3–15, 2005.

[9] E. Glover, C.-C. Chang, D. Gorinevsky, and S. Lall. Frequency stability for distributed generation connected through grid-tie inverter. In *IEEE POWERCON*, 2012.

[10] J. M. Guerrero, L. Garcia de Vicuna, J. Matas, M. Castilla, and J. Miret. A wireless controller to enhance dynamic performance of parallel inverters in distributed generation systems. *IEEE Transactions on Power Electronics*, 19(5):1205–1213, 2004.

[11] X. Guo, Z. Lu, B. Wang, X. Sun, L. Wang, and J. M. Guerrero. Dynamic phasors-based modeling and stability analysis of droop-controlled inverters for microgrid applications. *IEEE Transactions on Smart Grid*, 5(6):2980–2987, 2014.

[12] S. H. Lee, G. Son, and J. W. Park. Power management and control for grid-connected DGs with intentional islanding operation of inverter. *IEEE Transactions on Power Systems*, 28(2):1235–1244, 2013.

[13] J. A. Pecas Lopes, C. L. Moreira, and A. G. Madureira. Defining control strategies for microgrids islanded operation. *IEEE Transactions on Power Systems*, 21(2):916–924, 2006.

[14] R. Majumder, B. Chaudhuri, A. Ghosh, R. Majumder, G. Ledwich, and F. Zare. Improvement of stability and load sharing in an autonomous microgrid using supplementary droop control loop. *IEEE Transactions on Power Systems*, 25(2):796–808, 2010.

[15] V. Mariani, F. Vasca, and J. M Guerrero. Analysis of droop controlled parallel inverters in islanded microgrids. In *IEEE International Energy Conference*, 2014.

[16] European Network of Transmission System Operators for Electricity. Network code for requirements for grid connection applicable to all generators, 2013.

[17] C. K. Sao and P. W. Lehn. Autonomous load sharing of voltage source converters. *IEEE Trans. on Power Delivery*, 20(2):1009–1016, 2005.

[18] T. L. Vandoorn, J. D. M. D. Kooning, B. Meersman, J. M. Guerrero, and L. Vandevelde. Automatic power-sharing modification of p/f droop controllers in low-voltage resistive microgrids. *IEEE Transactions on Power Delivery*, 27(4):2318–2325, 2012.

[19] W. Yao, M. Chen, J. Matas, J. M. Guerrero, and Z. M. Qian. Design and analysis of the droop control method for parallel inverters considering the impact of the complex impedance on the power sharing. *IEEE Transactions on Industrial Electronics*, 58(2):576–588, 2011.

APPENDIX

Section VI-A claims that $|\varphi_{N_k} - \varphi_{N_j}|$ and $|\varphi_{N_k}|$ are small for all k, j for the distribution system with linear topology shown in Figure 6. Below, this assumption is analyzed quantitatively from the perspective of power consumption.

Let $V_{G_k} = |V_{G_k}| \angle \varphi_{G_k}$ for $k = 1, 2, \ldots, m$, and let $a_k = \varphi_{G_{k+1}} - \varphi_{G_k}$ with the convention that $\varphi_{G_{m+1}} = \angle V_G = 0$. Define l_k to be the length of the line between V_{G_k} and $V_{G_{k+1}}$. Let Z_0 be the impedance of the distribution line per unit length, so that $Z_{MV_k} = l_k Z_0$.

By the Cauchy-Schwarz Inequality we have

$$\left(\sum_{k=1}^{m} a_k \right)^2 \leq \left(\sum_{k=1}^{m} \frac{a_k^2}{l_k} \right) \cdot \left(\sum_{k=1}^{m} l_k \right). \tag{42}$$

Note that $\sum_{k=1}^{m} a_k = -\varphi_{G_1}$ and

$$\sum_{k=1}^{m} \frac{a_k^2}{l_k} = \frac{Z_0^*}{|V_G|^2} \sum_{k=1}^{m} \frac{|V_G|^2 a_k^2}{l_k Z_0^*} \approx \frac{Z_0^*}{|V_G|^2} \underbrace{\sum_{k=1}^{m} \frac{|V_{G_{k+1}} - V_{G_k}|^2}{Z_{G_k}^*}}_{S_{MV}},$$

where S_{MV} is the total complex power over the distribution line, which has the same phase angle as Z_0. Let $l = \sum_{k=1}^{m} l_k$ and $Z_{MV} = l Z_0$. Then,

$$|\varphi_{G_1}|^2 \leq S_{MV} \frac{Z_{MV}^*}{|V_G|^2} = |S_{MV}| \frac{|Z_{MV}|}{|V_G|^2}, \tag{43}$$

where Z_{MV} and S_{MV} have the same phase angle. In normal operation, the complex power over the line, $|S_{MV}|$, is small so $|\varphi_{G_1}|$ is also small. The same holds for $|\varphi_{G_k}|$, $k = 2, \ldots, m$.

We consider the circuit between V_{G_k} and the customer k. Using the single inverter model of Section III, we can similarly show that $|\varphi_{N_k} - \varphi_{G_k}|$ is small, that is,

$$|\varphi_{N_k} - \varphi_{G_k}|^2 \approx |S_{LV,k}| \frac{|Z_{LV,k}|}{|V_G|^2}, \tag{44}$$

where $S_{LV,k}$ is the complex power over the LV grid k. Hence, by the triangle inequality $|\varphi_{N_k}|$ is also small,

$$|\varphi_{N_k}| \leq |\varphi_{N_k} - \varphi_{G_k}| + |\varphi_{G_k}|, \tag{45}$$

where the upper bound is given by (43), (44), and (45). One can use similar upper bound to show that $|\varphi_{N_i} - \varphi_{N_j}|$ is small for any $i, j \in \{1, 2, \ldots, m\}$.

Chung-Ching Chang (S'01–M'14) received the B.S. degree in Electrical Engineering from National Taiwan University, Taipei, Taiwan, in 2003, and M.S. and Ph.D. degrees from Stanford University, Stanford, CA, USA in 2007 and 2013, respectively. His research interests include control, signal processing, optimization, and machine learning, with applications in the smart grid, distributed systems, and computer vision. This work was completed when he was at Stanford. He is presently with Google.

Dimitry Gorinevsky (M'91–SM'98–F'06) received a Ph.D. from Department of Mechanics and Mathematics at Moscow (Lomonosov) University in 1986, and a M.Sc. from Moscow Institute of Physics and Technology (Fiztech) in 1982. He is a Consulting Professor in Electrical Engineering at Stanford University and leads Mitek Analytics LLC consultancy in Palo Alto, CA. In the past, he spent 10 years with Honeywell. He worked on decision and control systems application across several industries. His current interests are in data analytics for industrial applications. Dr. Gorinevsky received Control Systems Technology Award, 2002, and Transactions on Control Systems Technology Outstanding Paper Award, 2004, of the IEEE Control Systems Society. He received Best Paper Award (Senior Award), 2013, of the IEEE Signal Processing Society.

Sanjay Lall (M'92–SM'06) is Associate Professor of Electrical Engineering in the Information Systems Laboratory and Associate Professor of Aeronautics and Astronautics at Stanford University. He received a B.A. degree in Mathematics with first-class honors in 1990 and a Ph.D. degree in Engineering in 1995, both from the University of Cambridge, England. His research group focuses on control, optimization and signal processing algorithms which occur in a wide variety of electrical, mechanical and aerospace systems. Before joining Stanford he was a Research Fellow at the California Institute of Technology in the Department of Control and Dynamical Systems, and prior to that he was a NATO Research Fellow at Massachusetts Institute of Technology, in the Laboratory for Information and Decision Systems. He was also a visiting scholar at Lund Institute of Technology in the Department of Automatic Control.